

## AlGa<sub>N</sub> Deep-Ultraviolet Light-Emitting Diodes

Jianping ZHANG\*, Xuhong HU, Alex LUNEV, Jianyu DENG, Yuriy BILENKO, Thomas M. KATONA, Michael S. SHUR, Remis GASKA and M. Asif KHAN<sup>1</sup>

*Sensor Electronic Technology, Inc., 1195 Atlas Rd., Columbia, SC 29209, U.S.A.*

<sup>1</sup>*Department of Electrical Engineering, University of South Carolina, Columbia, SC 29208, U.S.A.*

(Received February 23, 2005; accepted June 30, 2005; published October 11, 2005)

We report on the development of AlGa<sub>N</sub> based deep ultraviolet (DUV) light-emitting diodes (LEDs) grown by migration-enhanced metalorganic chemical vapor deposition (MEMOCVD). Improved quality of AlGa<sub>N</sub> has allowed us to achieve milliwatt-power at wavelengths ranging from 365 to 265 nm. For 295 and 280 nm LEDs, record CW powers with wall-plug-efficiency approaching 1.0% were realized. The CW power reached 1.2 and 1.0 mW at 20 mA for 280 and 295 nm LEDs, respectively. A multiple-chip package (UV lamp) emitted CW power of 11 mW at the wavelength of 280 nm. Under pulse operation, the 280 nm UV lamp produced power as high as 56 mW. The CW power levels at 20 mA were 0.5, 0.25 and 0.15 mW for a single-chip 275, 270 and 265 nm LEDs, respectively. A 265 nm UV lamp exhibited a record high CW power exceeding 1.5 mW. The applications of these DUV LEDs in bio-agents detection have been demonstrated and the preliminary results will be presented. [DOI: 10.1143/JJAP.44.7250]

KEYWORDS: AlGa<sub>N</sub>, Deep UV LEDs, MOCVD, Bio-fluorescence

### 1. Introduction

High-efficiency compact environmentally-friendly solid-state deep ultraviolet (DUV) light sources could replace the conventional mercury lamps and find numerous applications in food/water sterilization, bio-agents detection, medicine, and covert non-line-of-sight communications. The group-III nitride semiconductors are the most suitable material system for DUV light emitters with the direct bandgap covering the whole UV spectrum except for the vacuum UV region. The past several years have witnessed a great deal of efforts to develop nitride-based DUV light emitting diodes (LEDs). Starting from April 2002 with the debut of the very first DUV LED operating in the UVC region (285 nm), with only a few tens of microwatt continuous-wave (CW) power,<sup>1,2</sup> many innovations in growth, processing and packaging have resulted in the recent high-efficiency 280 nm LEDs, with CW powers exceeding 1.0 mW at 20 mA.<sup>3,4</sup> Among these innovations, results to date for sub-290 nm DUV LEDs<sup>3–12</sup> indicate that high-temperature thick AlN buffers and strain-management/defect-filtering AlN/AlGa<sub>N</sub> superlattices<sup>13–16</sup> are crucial for obtaining high-performance devices. The employment of migration-enhanced metalorganic chemical vapor deposition (MEMOCVD)<sup>15,16</sup> to the growth of the AlN and AlN/AlGa<sub>N</sub> superlattices was the key to obtaining these milliwatt high powers. Meanwhile, other approaches have also been investigated to produce efficient UV LEDs. Nikishin *et al.* used short-period superlattices to replace AlGa<sub>N</sub> alloys<sup>17</sup> and Kim *et al.* used very thick AlN templates for UV LED growths.<sup>18</sup>

In this paper, we will report our results on AlGa<sub>N</sub> based DUV LEDs with emission wavelengths  $\lambda < 300$  nm. Record-high CW powers of 11 and 1.5 mW were achieved for 280 and 265 nm LEDs, respectively. In the pulse regime, the respective powers reached 56 and 10 mW. The preliminary device reliability data and applications to bio-detection will also be presented.

### 2. Growth

All the LED structures were grown on basal-plane sapphire substrates using a custom-designed vertical metalorganic chemical vapor deposition (MOCVD) system. Trimethyl aluminum (TMA), trimethyl gallium (TMG), trimethyl indium (TMI), silane, Cp2-Mg, and NH<sub>3</sub> were used as precursors. The device structures for different wavelengths are similar (except for the Al molar fractions). As seen in Fig. 1 and also reported previously,<sup>3,5,6</sup> the structure features a high-temperature AlN buffer layer and an AlN/AlGa<sub>N</sub> superlattice grown by the MEMOCVD,<sup>15</sup> with the precursor pulse durations and overlaps optimized to achieve the highest quality. These layers are followed by a 3–4- $\mu$ m-thick Si-doped AlGa<sub>N</sub>, a multiple-quantum-well (MQW) active region, a Mg-doped p-AlGa<sub>N</sub> blocking layer, and a graded p-AlInGa<sub>N</sub> p-contact layer. The detailed material characterizations including Hall-effect measurement, symmetric and asymmetric X-ray single scans and maps, photoluminescence, and atomic force microscopy were performed to evaluate the effect of the MEMOCVD-grown AlN buffer and AlN/AlGa<sub>N</sub> superlattice on the n-AlGa<sub>N</sub> material quality.<sup>14,16</sup> The AlN/AlGa<sub>N</sub> superlattice

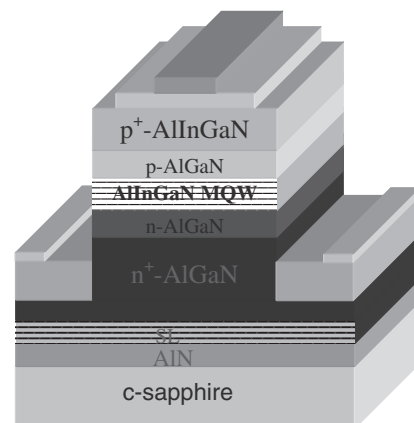


Fig. 1. Schematics of AlGa<sub>N</sub> DUV LED structure.

\*E-mail address: jp@s-et.com

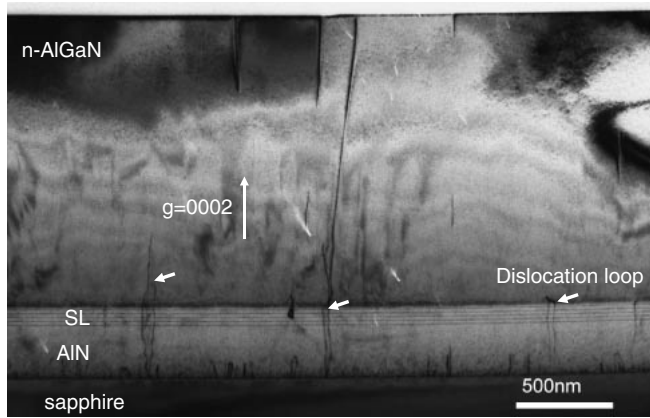


Fig. 2. Cross-section TEM ( $g = 0002$ ) showing the buffer structure of our 280 nm LED. The diffraction geometry reveals screw dislocations in the structure. Note the effective reduction in screw-dislocation density ( $3 \times 10^8 \text{ cm}^{-2}$ ) achieved by MEMOCVD and dislocation loop formation (short arrows) after the superlattice.

were found to enlarge the n-AlGaIn mosaic block dimensions, which, in turn, reduced the tensile strain resulting from the fine-grain structure.<sup>14</sup> The MEMOCVD had two main benefits: enhancing the surface migration of the growth species and reducing the gas-phase reaction. These improvements reduced the screw-dislocation density. Figure 2 shows the cross-section transmission-electron-microscopic (TEM) micrograph of the buffer structure of our 280 nm LED. The chosen diffraction geometry [ $g = (0002)$ ] reveals the screw dislocations in the structure. As seen, the screw-dislocation density is around  $3 \times 10^8 \text{ cm}^{-2}$ , starting approximately 100 nm apart from the AlN/sapphire interface. This number should be compared to the screw-dislocation density of the mid- $10^{10} \text{ cm}^{-2}$ , commonly observed in the conventional MOCVD grown AlN layers. This confirms that MEMOCVD is very efficient in reducing the screw-dislocation density. The dislocation loops formed just above the superlattice imply that the superlattice enhanced the n-AlGaIn mosaic block dimensions via the dislocation annihilation, as measured in ref. 14. A TEM study also showed that MEMOCVD and the superlattice had much less effect on the edge-dislocation density. Improved growth techniques which could reduce edge-dislocation density are expected to increase the DUV LED efficiency.

### 3. Processing

LEDs were processed with the standard steps, including photolithography, dry etching, and metal evaporation. Mesa structures (as shown in Fig. 1, the effective device area was  $100 \times 100 \mu\text{m}^2$ ) were etched using chlorine-plasma reactive ions. Ti/Al/Ti/Au n-type ohmic contact metals were annealed in flowing forming gas at  $850\text{--}950^\circ\text{C}$ , depending on the n-AlGaIn Al-composition. Ni/Au metals were used for p-contact metallization (annealed at  $500^\circ\text{C}$ ). The transfer length measurements (TLM) were performed to assert the contact quality. The bottom thick n-AlGaIn sheet resistances, derived from the n-TLM measurements, ranged from  $140$  to  $260 \Omega/\square$  for 295 to 265 nm LED wafers, respectively. The n- and p-type specific contact resistances were around  $1.0 \times 10^{-5}$  and  $1.0 \times 10^{-4} \Omega \text{ cm}^2$  for these wavelengths LEDs, respectively. Figure 3 shows a representative current–volt-

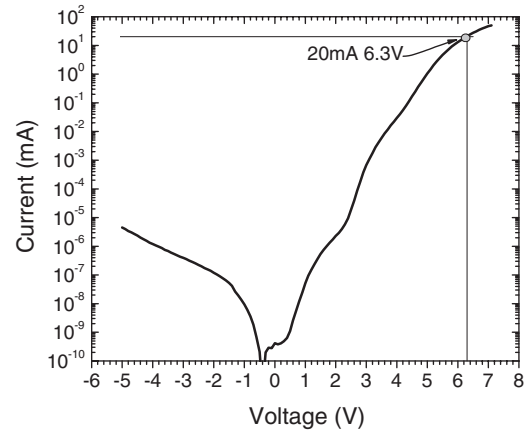


Fig. 3. A representative  $I$ – $V$  curve for 280 nm LED.

age ( $I$ – $V$ ) curve for our 280 nm LEDs. At  $-5 \text{ V}$  reverse bias, the device leakage current was approximately 5 nA. The forward operating voltage at 20 mA was 6.3 V. The device forward characteristics indicated a behavior typical of several connected diodes. The parasitic diodes might arise from the non-ohmic p-contacts and/or from p-GaN/p-AlGaIn interfaces.

The LED chips were then diced and flip-chip packaged in commercial TO39 headers with AlN ceramic heat sinks. Single-chip (LEDs) and multiple-chip devices (lamps) were packaged for different direct current (DC) operation. A UV lamp usually contains three chips connected in parallel.

### 4. Device Performance

The LED characteristics measured at room-temperature (RT) included electroluminescence (EL) spectra, CW and pulse powers, and preliminary reliability tests. In Fig. 4, we present the typical EL spectra of our 265–295 nm LEDs. Superior spectral purity was evidenced in all the LEDs, with the main-peak/background intensity ratios being well above 2000. The peak full width at half maximum (FWHM) value was typically below 10 nm. To investigate the emission mechanism, the EL spectra were recorded in a wide range of current densities, from  $50 \text{ A/cm}^2$  to  $4 \text{ kA/cm}^2$ , corresponding to the currents of 5 to 400 mA. The current was switched to pulse mode for high injection ( $I \geq 50 \text{ mA}$ ), with a duty cycle of 1% and repetition rate of 1 kHz. Shown in Fig. 5(a) are the EL spectra at different current levels. Figure 5(b)

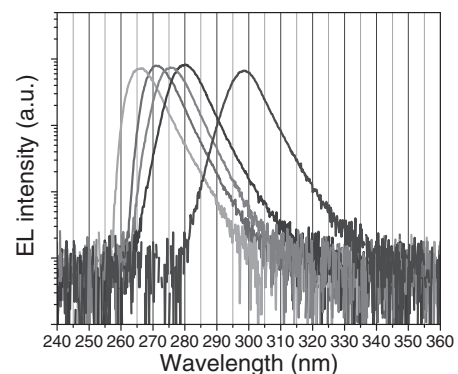


Fig. 4. Electroluminescence spectra of DUV LEDs with peak emission at 265, 270, 275, 280, and 295 nm, respectively.

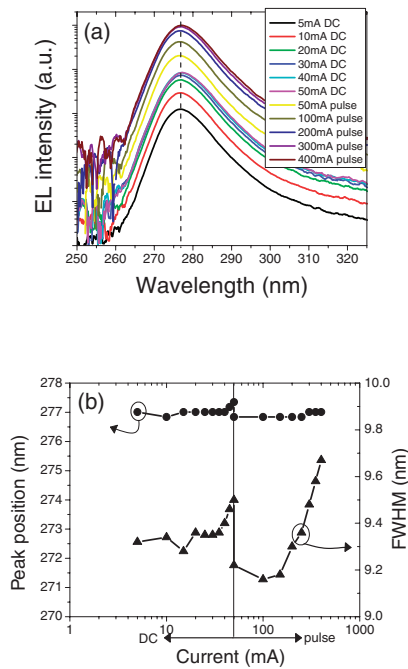


Fig. 5. (a) Electroluminescence spectra of 277 nm LEDs under different currents, for current  $\geq 50$  mA, pulse currents with duty cycle of 1% frequency of 1 kHz were used. (b) Emission peak position and spectral width as a function of current.

shows the emission peak position and FWHM data as a function of the injected current. Under small DC injection, the EL peak showed a slight red shift with increasing current density. This red shift is believed to be mainly due to the heat-related bandgap shrinkage. Under higher current injection (which was done in the pulse regime so that heating was avoided), the peak position did not show redshift (within the measurement error) [see Fig. 5(b)]. The small spectral broadening with increasing injection [seen in Fig. 5(b)] is related to both heating and band filling. In InGaN visible LEDs a strong spectral blueshift is commonly observed when current density increases in the low injection regime. The absence of the strong blueshift in our devices indicates that the emission was of quantum-well nature, as opposed to the band-tail or quantum-dot mechanism, which is invoked to explain the InGaN-based visible LED characteristics.

In Fig. 6, we summarized our single-chip LEDs CW powers for different wavelengths. All the power measurements were done in an integration sphere. As seen, milliwatt-level LEDs in the 275–295 nm region with small DC driving have been achieved, though the efficiency dropped for shorter wavelengths. A close inspection of the EL spectra shown in Fig. 4 revealed that the 265, 270, 275-nm LEDs had strong self-absorption on the high-energy side. Increasing the Al molar fraction in the bottom n-AlGaIn layer could reduce this self-absorption and increase those LED power levels. However, a tradeoff must be established between the transparency and the n-type conduction. New experiments will be undertaken to optimize these LEDs powers. For 280–295 nm LEDs, the spectra were fairly symmetric and milliwatt powers were produced at current as small as 20 mA.

In order to gain higher CW power, three chips were connected in parallel to form UV lamps. Figure 7 presents the CW/pulse powers from our 265 and 280 nm UV lamps.

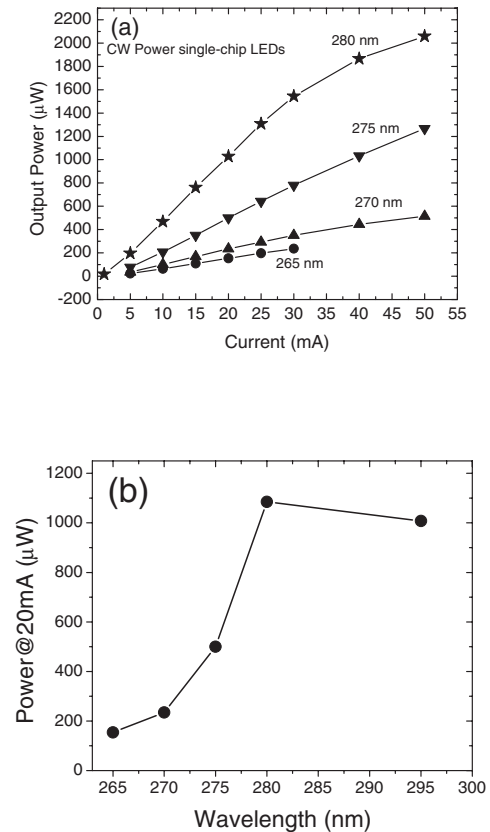


Fig. 6. (a) CW power-current plot for 265, 270, 275, and 280 nm single-chip packaged LEDs, respectively. (b) Plot of power at 20 mA DC vs. emission wavelength.

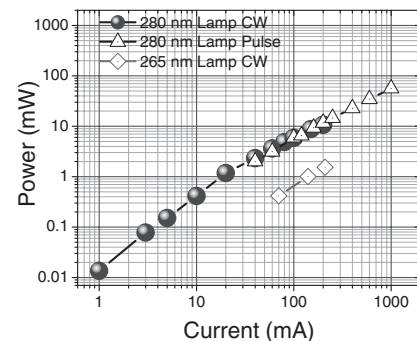


Fig. 7. Power-current plot for 265 and 280 nm DUV lamps (three chips connected in parallel). In the pulse measurement, a duty cycle of 2% and a repetition rate of 10 kHz were used. Solid circles: 280 nm CW powers; open triangles: 280 nm pulse powers; open diamonds: 265 nm CW powers.

The CW power exceeding 1.5 mW was measured for the 265 nm UV lamp. The 280 nm lamp emitted 11 mW CW power at 200 mA. Under pulse operation, (with the duty cycle of 2% and the repetition rate of 10 kHz), the power in excess of 56 mW for 280 nm emission was achieved.

Preliminary reliability tests of these DUV LEDs showed that the devices were fairly stable for the operations at relatively small current densities. For 280 nm LEDs, the power degradation mainly occurred during the first 30 h (stressed under 200 A/cm<sup>2</sup>). The power remained constant (70% of the initial power) for the rest of test (over 300 h). Future accelerated lifetime measurements might reveal the mechanisms determining the device reliability.

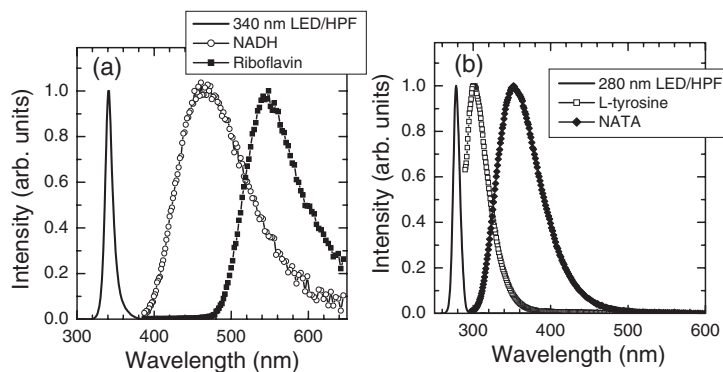


Fig. 8. (a) Normalized fluorescence spectra of NADH (open circles), and riboflavin (solid squares) under 340-nm LED excitation (solid line). (b) Normalized fluorescence spectra of L-tyrosine (open squares) and tryptophane derivative NATA (solid diamonds) under 280-nm LED excitation (solid line). The LEDs are equipped with high-pass filters (HPFs) to remove any possible residual long-wavelength emissions.

## 5. DUV LED Application Demonstration

One of the key applications of the DUV LEDs uses the deep UV germicidal effect and fluorescence. Owing to small dimensions and weight, low power consumption, stability, and low cost, DUV LEDs are excellent candidates for many fluorescence sensor applications, such as point-of-care medical diagnostics or detection of hazardous biological compounds and agents. We have reported on the high-frequency modulation of 340-nm and 280-nm LEDs up to 200 MHz and the application of these sources for frequency-domain fluorescence lifetime measurements in four basic biological autofluorophores, namely coenzymes nicotinamide adenine dinucleotide (NADH), riboflavin, aromatic amino acids tyrosine, and tryptophane.<sup>19</sup> As an example, Fig. 8 shows the fluorescence spectra for the four basic bioautofluorophores, excited by our 340 and 280 nm LEDs. The LEDs were equipped with high-pass filters (HPFs) to remove any possible residual long-wavelength emissions. The 340-nm LEDs were used for the characterization of coenzymes NADH and riboflavin, whereas the 280-nm devices were used to excite fluorescence in derivatives of aromatic amino acids tyrosine and tryptophane (NATA). The spectra show typical broad fluorescence bands peaked at 301 nm for L-tyrosine, 355 nm for NATA, 465 nm for NADH, and 545 nm for riboflavin, respectively, with reasonable intensities and relatively low noise levels.

## 6. Conclusion

In conclusion, milliwatt-level power deep UV LEDs operating in the UVC region ( $\lambda < 300$  nm) have been demonstrated. 280 nm, 295 nm LEDs with CW power exceeding 1 mW at 20 mA (with wall-plug-efficiency approaching 1%) were reported. The UV lamps produced CW power in excess of 1.5 mW at 265 nm, 11 mW at 280 nm, and pulse power over 56 mW at 280 nm. Preliminary reliability tests showed that the devices were fairly stable under low current-density operation. The applicability of DUV LEDs in biosensing/biofluorescence has been demonstrated.

## Acknowledgement

The work on deep UV LED development at Sensor Electronic Technology, Inc. was supported by DARPA (Program Manager Dr. John Carrano). We cordially thank

Professor Fernando Ponce (Arizona State University) for the TEM result (Fig. 2) and Dr. Michael Wraback and Dr. Charles Collins (US Army Research Lab) for some of the electroluminescence measurements (Fig. 5).

- 1) V. Adivarahan, J. P. Zhang, A. Chitnis, W. Shuai, J. Sun, R. Pachipulusu, M. Shatalov and A. Khan: *Jpn. J. Appl. Phys.* **41** (2002) L435.
- 2) V. Adivarahan, S. Wu, A. Chitnis, R. Pachipulusu, V. Mandavilli, M. Shatalov, J. P. Zhang, M. A. Khan, G. Tamulaitis, A. Sereika, I. Yilmaz, M. S. Shur and R. Gaska: *Appl. Phys. Lett.* **81** (2002) 3666.
- 3) J. P. Zhang, X. Hu, Y. Bilenko, J. Deng, A. Lunev, R. Gaska, M. Shatalov, J. W. Yang and M. A. Khan: *Appl. Phys. Lett.* **85** (2004) 5532.
- 4) W. H. Sun, V. Adivarahan, M. Shatalov, Y. Lee, S. Wu, J. W. Yang, J. P. Zhang and M. A. Khan: *Jpn. J. Appl. Phys.* **43** (2004) L1419.
- 5) J. P. Zhang, A. Chitnis, V. Adivarahan, S. Wu, V. Mandavilli, R. Pachipulusu, M. Shatalov, G. Simin, J. W. Yang and M. A. Khan: *Appl. Phys. Lett.* **81** (2002) 4910.
- 6) J. P. Zhang, S. Wu, S. Rai, V. Mandavilli, V. Adivarahan, A. Chitnis, M. Shatalov and M. A. Khan: *Appl. Phys. Lett.* **83** (2003) 3456.
- 7) V. Adivarahan, S. Wu, J. P. Zhang, A. Chitnis, M. Shatalov, V. Mandavilli, R. Gaska and M. A. Khan: *Appl. Phys. Lett.* **84** (2004) 4762.
- 8) W. H. Sun, J. P. Zhang, V. Adivarahan, A. Chitnis, M. Shatalov, S. Wu, V. Mandavilli, J. W. Yang and M. A. Khan: *Appl. Phys. Lett.* **85** (2004) 531.
- 9) A. Yasan, R. McClintock, K. Mayes, D. Shiell, L. Gautero, S. R. Darvish, P. Kung and M. Razeghi: *Appl. Phys. Lett.* **83** (2003) 4701.
- 10) K. Mayes, A. Yasan, R. McClintock, D. Shiell, S. R. Darvish, P. Kung and M. Razeghi: *Appl. Phys. Lett.* **84** (2004) 1046.
- 11) A. J. Fischer, A. A. Allerman, M. H. Crawford, K. H. A. Bogart, S. R. Lee, R. J. Kaplar, W. W. Chow, S. R. Kurtz, K. W. Fullmer and J. J. Figiel: *Appl. Phys. Lett.* **84** (2004) 3394.
- 12) A. Hanlon, P. M. Pattison, J. F. Kaeding, R. Sharma, P. Fini and S. Nakamura: *Jpn. J. Appl. Phys.* **42** (2003) L628.
- 13) J. P. Zhang, H. M. Wang, M. E. Gaevski, C. Q. Chen, Q. Fareed, J. W. Yang, G. Simin and M. A. Khan: *Appl. Phys. Lett.* **80** (2002) 3542.
- 14) H. M. Wang, J. P. Zhang, C. Q. Chen, Q. Fareed, J. W. Yang and M. A. Khan: *Appl. Phys. Lett.* **81** (2002) 604.
- 15) J. P. Zhang, M. A. Khan, W. H. Sun, H. M. Wang, C. Q. Chen, Q. Fareed, E. Kuokstis and J. W. Yang: *Appl. Phys. Lett.* **81** (2002) 4392.
- 16) J. P. Zhang, H. M. Wang, W. H. Sun, V. Adivarahan, S. Wu, A. Chitnis, C. Q. Chen, M. Shatalov, E. Kuokstis, J. W. Yang and M. A. Khan: *J. Electron. Mater.* **32** (2003) 364.
- 17) S. A. Nikishin, V. V. Kuryatkov, A. Chandolu, B. A. Borisov, Gela D. Kipshidze, I. Ahmadi, M. Holtzl and H. Temkin: *Jpn. J. Appl. Phys.* **42** (2003) L1362.
- 18) K. H. Kim, Z. Y. Fan, M. Khizar, M. L. Nakarmi, J. Y. Lin and H. X. Jiang: *Appl. Phys. Lett.* **85** (2004) 4777.
- 19) P. Vitta, N. Kurilcik, A. Novickovas, S. Jursenas, H. Calkauskas, A. Zukauskas and R. Gaska: *Proc. SPIE* **5617** (2004) 249.